# On Wave Force Analysis Using System Identification

K Worden, P K Stansby and G R Tomlinson
Department of Engineering
The University
Oxford Road
Manchester
M13 9PL

S A Billings
Department of Automatic Control and Systems Engineering
University of Sheffield
P O Box 600
Mappin Street
Sheffield
S1 4DU

Research Report No 450

April 1992

# On Wave Force Analysis Using System Identification.

K.Worden P.K.Stansby G.R.Tomlinson
Department of Engineering
The University
Oxford Road
Manchester M13 9PL

S.A.Billings
Department of Automatic Control and Systems Engineering
University of Sheffield
Mappin Street
Sheffield S1 3JD

**Abstract**

It is well known that the Morison equation has a limited capability in predicting wave forces on slender cylindrical members of offshore structures. Attempts have been made to improve prediction in both the time and frequency domains using system identification. In this paper the work to date will be reviewed. System identification requires samples of time data for force and flow velocity; considered here are data from a U-tube, the De Voorst wave flume and the Christchurch Bay tower. The results obtained in the time-domain include an improved classification of wave forces and excellent predictions of measured forces although the model structures are case specific. A series expansion for the force spectrum is proposed via the Morison-Duffing equation which promises more accurate modelling of high frequency components in the force histories for general application. This has implications for fatigue analysis.

## 1 Introduction

Since its introduction in 1950 [11], the Morison equation has provided the main means of predicting wave forces on slender cylinders. In the usual notation,

$$F = \frac{1}{2}\rho D C_d u|u| + \frac{1}{4}\pi\rho D^2 C_m \dot{u} \tag{1}$$

where $F(t)$ is the force per unit axial length, $u(t)$ is the instantaneous flow velocity, $\rho$ is water density and $D$ is diameter. The dimensionless drag and inertia coefficients $C_d$ and $C_m$ depend on the characteristics of the flow. In general the main dependence is taken to be on $Re$, the Reynolds number, and $KC$, the Keulegan-Carpenter number although these parameters do not have generally accepted definitions in random or directional waves. In place of $Re$, the Stokes parameter $\beta = Re/KC$ is often used. The coefficients $C_d$ and $C_m$ are usually obtained by applying least-squares procedures to measured force and velocity data.

It is well known that Morison's equation has deficiencies, particularly in the $KC$ range 8 to 20 when vortex shedding effects from the cylinder are very significant. This manifests itself as an inability to model the high frequency components of the force; this has serious implications for fatigue studies.

The aim of the present work was to determine whether improvements on the Morison equation could be obtained which would produce better predictions of force time-histories measured in a variety of flow situations, ranging from sinusoidal flow in a U-tube, to unidirectional random waves in a large wave flume, to directional seas in Christchurch Bay. Previous work in this area seems to have been restricted to the addition of velocity-based terms to Morison's equation in order to improve predictions for U-tube data [15].

Section two describes how additional terms for the Morison equation have been hypothesised on physical grounds and it is described how even a single additional term, $F|F|$, significantly improves curve fits. This allows an improved classification into drag, inertia and history.

Unfortunately the new equation does not improve prediction due to its stability characteristics. In section three, NARMAX nonlinear time series techniques are described, which give a model structure automatically in discrete-time form. The models are shown to satisfy strict validity criteria. The NARMAX models give good curve-fits *and* predictions but the equation structures vary from one flow situation to another.

In section four it is shown how the NARMAX models may be used to generate higher order frequency response functions (FRFs). Consistent structure is seen for all the flows in the third order FRFs (Second order effects are always small). This structure is completely different from that obtained from the Morison equation. Also, closed form expressions for the nonlinear FRFs are obtained in order to examine quantitatively the variation in structure from one flow to another. Preliminary results are presented.

Finally, the use of neural network models is briefly discussed and again some preliminary results are presented.

## 2 Improved Wave Force Classification

It is well known that the time-history of the wave-force on a cylinder can be due to complicated flow effects which differ from one situation to another. If the Morison equation is to predict accurately, all nonlinear effects must be represented by the nonlinear 'drag' term proportional to $u|u|$. The linear inertia component is in part due to the inviscid effect of flow acceleration. Expansion of the drag term as a polynomial gives

$$u|u| = a_1 u + a_3 u^3 + a_5 u^5 \ldots \tag{2}$$

which shows that even if the flow velocity is a sinusoid $u(t) = U_0 \sin(2\pi t/T)$ the force signal will contain all odd harmonics. One immediately sees that the explanation for the failure of Morison's equation to predict the higher frequency behaviour of the force signal is that the relative size of *all* harmonic components must be fixed by the one coefficient $C_d$.

A more detailed discussion of the physics of the situation is given in [16], briefly, the rate at which vorticity is shed at separation is equal to $\pm\frac{1}{2}u_s^2$, where $u_s$ is the velocity just outside the boundary layer at separation. $u|u|$ is thus roughly proportional to the rate of shedding of vorticity and the drag term in Morison's equation may be associated with this effect.

Since the drag term is associated with vorticity generation and the history of vortex shedding can be a significant effect, one might expect the additional influence of vortex shedding on force to be modelled by higher order and time derivative terms in $F$. As a further rationale, it is common practice in system identification to include output terms to model history effects in order to produce a parsimonious model. Initially additional terms proportional to $F^2$, $F^3$, $\dot{F}$ and $\ddot{F}$ were included which are in fact the terms in the equation for the Duffing oscillator. After some preliminary tests on U-tube data it became apparent that the $F^2$ term could be discarded as insignificant; the model also showed a degree of improvement when the $F^3$ term was replaced by one with the form $F|F|$. The form of the extended Morison equation or Morison-Duffing equation is thus

$$\alpha_1\ddot{F} + \alpha_2\dot{F} + F + \alpha_3 F|F| = \frac{1}{2}\rho D C_d u|u| + \frac{1}{4}\pi\rho D^2 C_m \dot{u} \tag{3}$$

The parameter estimation technique which enabled the determination of the coefficients $\alpha_1$, $\alpha_2$, $\alpha_3$, $C_d$ and $C_m$ which give the best fit to the measured data are described in [16]. The relative importance of the new terms can also be established. We refer to these extra terms as 'history' terms although the drag and inertia inevitably contain history effects also. However, the additional terms are specifically included to model the 'gross' history effect of vortex shedding.

While one aim is to improve force prediction, another is to improve force classification by improving the fit of the equation to the measured data. With the Morison equation, estimates of $C_d$ and $C_m$ are biased by the residual error which has a structure determined by the flow mechanisms. The history terms should improve the fit and therefore give improved estimates of the contribution from drag, inertia and history.

Having obtained a set of model parameters, it is necessary to check the accuracy of the model. The simplest means of doing this is to plot and compare the measured force $F_i$ at each sampling instant with the curve-fit value

$$\hat{F}_i = -\alpha_1\ddot{F}_i - \alpha_2\dot{F}_i - \alpha_3 F_i|F_i| + \beta_1 u_i|u_i| + \beta_2\dot{u}_i \tag{4}$$

based on the estimated parameters. $\beta_1$ and $\beta_2$ have been introduced in order to simplify the notation. One can also use a numerical measure of the closeness of fit; the measure adopted here is the normalised mean-square error or $MSE$ defined by

$$MSE(\hat{F}) = \frac{100}{N\sigma_F^2}\sum_{i=1}^{N}(F_i - \hat{F}_i)^2 \tag{5}$$

This $MSE$ has the following useful property; if the mean of the force signal $\overline{F}$ is used as the model i.e. $\hat{F}_i = \overline{F}$ for all $i$, the $MSE$ is 100%.

A more stringent test of the model validity is to predict the wave force from equation (3) using measured velocities and accelerations only, via some time-stepping procedure. This can then be compared with the measured force. The fact that one needs to integrate a differential equation is a disadvantage of using a continuous-time model. A further problem is the fact that samples of $\dot{F}$ and $\ddot{F}$ data are required by the parameter estimation procedures; these need to be estimated by numerical differentiation. The estimated derivatives were found to be extremely senstive to noise on the $F$ data. In order to avoid these problems, the following discrete-time or NARMAX [9] version of (3) was adopted.

$$F_i = a_1 F_{i-1} + a_2 F_{i-2} + a_3 F_{i-1}|F_{i-1}| + b_1 u_{i-1} + b_2 u_{i-2} + b_3 u_{i-1}|u_{i-1}| \tag{6}$$

The measured data were obtained from three sources. In the first case, forces on a cylinder in the sinusoidal flow of a U-tube were obtained from the experiments of Obasaju *et al.* [12]. The data were obtained by digitising plots of force against time for $KC = 3.31, 6.48, 11.88, 17.5$ and $34.68$ available with $\beta = 417$. Forces were also measured on a cylinder oscillating in still water and a uniform current by Obasaju et.al. [13]. For the latter there is now an additional parameter defining the flow, the ratio of current velocity to the amplitude of the oscillatory velocity, $a$. In the situations with a current a single drag term in the Morison equation is maintained, i.e. an 'oscillatory' drag and 'current' drag are not considered separately.

The second source of data was the velocities and forces due to random waves on a fixed smooth cylinder measured in the Delta flume of the De Voorst facility of Delft Hydraulics. The waves were generated to give a JONSWAP surface elevation spectrum. Further details are given in [16].

The final source of data was forces and velocities measured on the Christchurch Bay Tower as described in [6]. The same cylinder was used in the De Voorst tests but the sea states have greater wave heights (up to 7m against 2m at De Voorst) and are directional with a prominent current.

Table 1 shows the results of fitting Morison's equation to the U-tube and De Voorst data. In addition to the fitted coefficients, the percentage contributions of the drag and inertia terms to the overall force signal are given.

| $KC$ | $\beta$ | $a$ | $C_d$ | $C_m$ | Drag % | Inertia % | $MSE$ % |
|---|---|---|---|---|---|---|---|
| Oscillatory flow data ( $KC = \frac{U_0 T}{D}$ ) | | | | | | | |
| 3.31 | 417 | 0.0 | 1.13 | 2.28 | 2 | 98 | 0.17 |
| 6.48 | 417 | 0.0 | 1.75 | 2.02 | 19 | 80 | 0.42 |
| 11.88 | 417 | 0.0 | 2.51 | 0.92 | 82 | 10 | 7.3 |
| 17.5 | 417 | 0.0 | 2.09 | 1.08 | 89 | 10 | 0.68 |
| 34.68 | 417 | 0.0 | 1.69 | 1.28 | 93 | 6 | 1.1 |
| 14.0 | 929 | 0.0 | 2.31 | 0.56 | 91 | 2 | 7.2 |
| 18.0 | 634 | 0.0 | 2.07 | 1.41 | 95 | 2 | 3.1 |
| 14.0 | 933 | 0.18 | 1.61 | 1.23 | 91 | 1 | 4.1 |
| 10.0 | 1081 | 0.52 | 1.38 | 1.24 | 81 | 1.5 | 5.8 |
| 14.0 | 417 | 1.01 | 1.23 | 1.58 | 74 | 2 | 0.38 |
| De Voorst ( $KC = \frac{\sqrt{2} u_{rms} T}{D}$ ) | | | | | | | |
| 5.03 | $\approx 4.10^4$ | 0.0 | 0.54 | 1.84 | 2.6 | 95 | 2.38 |

Table 1: Morison Fit to Data.

The curve-fit for the $KC = 11.88$ data is shown in Figure 1. The result is clearly inadequate.

When the Morison-Duffing equation was used for the curve fitting, the results showed an enormous improvement over the Morison equation, an example for $KC = 11.88$ is given in Figure 2. However, when the predicted force output was obtained from equation (6) by stepping $F_i$ forward in time using the measured velocities only and using $F_1$ and $F_2$ to start the calculation, the $MSE$ values showed

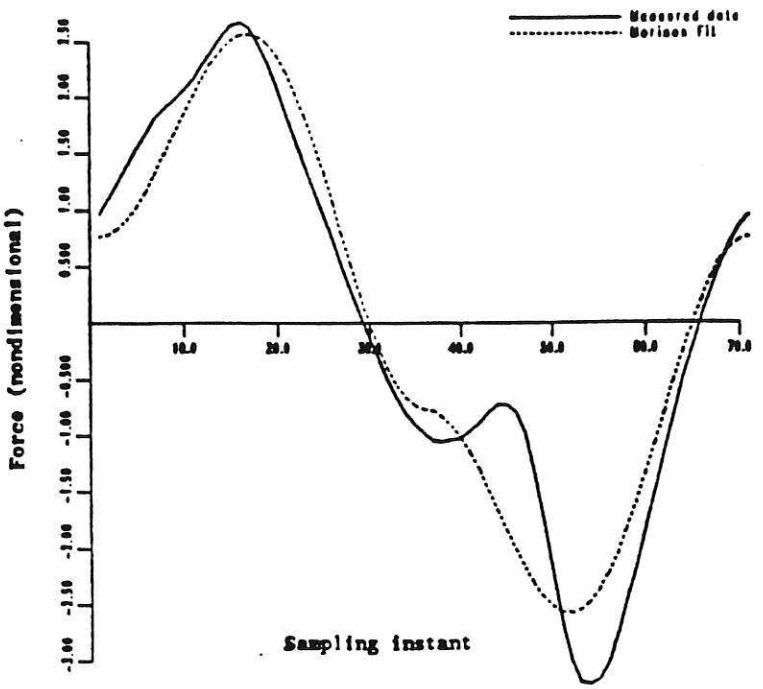


Figure 1. Comparison between measured U-tube data and Morison equation prediction. $KC = 11.88$.

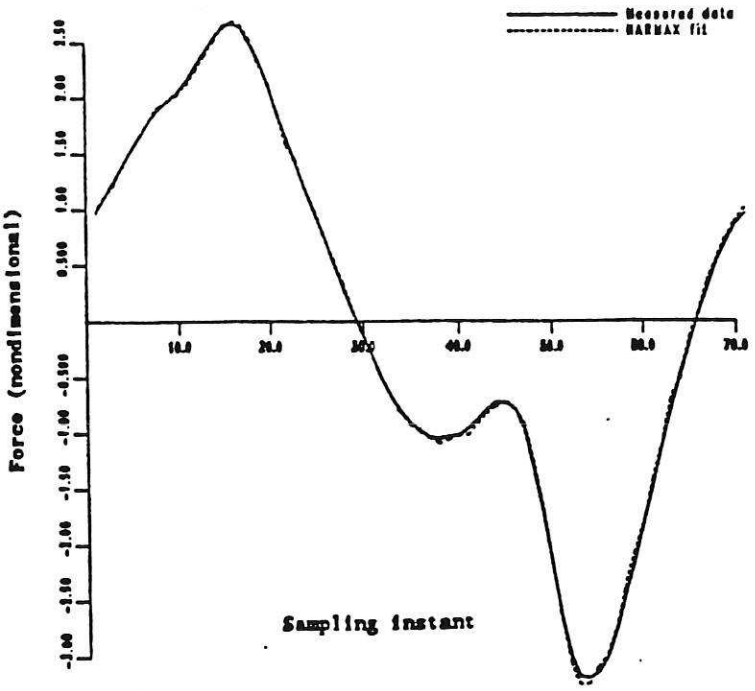


Figure 2. Comparison between measured data and least squares curve-fit for the Morison-Duffing equation.

no appreciable improvement over those for the Morison fit. This is a surprising result in view of the excellent curve fits and has yet to be properly understood.

The analysis indicated that the $F|F|$ term in equation (6) generally made the most significant contribution to the fit and an equation structure including only this extra term was tested:

$$F + \alpha F|F| = \beta_1 u|u| + \beta_2 \dot{u} \tag{7}$$

the results are given in Table 2.

| $KC$ | $\beta$ | $a$ | $C_d$ | $C_m$ | $\alpha$ | Drag % | Inertia % | History % | $MSE$ % |
|---|---|---|---|---|---|---|---|---|---|
| Oscillatory flow data ( $KC = \frac{U_0 T}{D}$ ) | | | | | | | | | |
| 3.31 | 417 | 0.0 | 1.09 | 2.18 | 0.01 | 1.8 | 89.6 | 0.2 | 0.17 |
| 6.48 | 417 | 0.0 | 1.42 | 1.59 | 0.07 | 12.4 | 49.8 | 4.6 | 0.18 |
| 11.88 | 417 | 0.0 | 1.25 | 0.64 | 0.22 | 20.5 | 5.1 | 26.7 | 2.2 |
| 17.5 | 417 | 0.0 | 1.85 | 0.99 | 0.06 | 69.7 | 8.6 | 1.3 | 0.59 |
| 34.68 | 417 | 0.0 | 1.40 | 1.12 | 0.12 | 63.5 | 4.6 | 3.2 | 0.75 |
| 14.0 | 929 | 0.0 | 1.23 | 0.79 | 0.21 | 25.6 | 0.5 | 25.7 | 1.7 |
| 18.0 | 634 | 0.0 | 1.45 | 1.32 | 0.17 | 46.9 | 0.9 | 9.3 | 2.3 |
| 14.0 | 933 | 0.18 | 0.93 | 1.18 | 0.57 | 30.0 | 0.7 | 18.3 | 2.2 |
| 10.0 | 1081 | 0.52 | 0.65 | 1.20 | 1.46 | 18.0 | 1.0 | 27.5 | 1.6 |
| 14.0 | 417 | 1.01 | 1.12 | 1.62 | 0.44 | 61.0 | 2.0 | 0.5 | 0.36 |
| De Voorst ( $KC = \frac{\sqrt{2} u_{rms} T}{D}$ ) | | | | | | | | | |
| 5.03 | $\approx 4.10^4$ | 0.0 | 0.46 | 1.55 | 0.07 | 1.87 | 67.0 | 2.8 | 2.0 |

Table 2: Morison $+\alpha F|F|$ Fit to Data.

The $MSE$'s are still significantly below the values for the Morison fits where the $MSE$ was high. In Table 2 the values of $\alpha$ are only meaningful when $F$ is normalised in some way. In this case this was achieved by dividing by $\frac{1}{2}\rho D U_0^2$ for sinusoidal flow and, equivalently, by $\rho D u_{rms}^2$ for the De Voorst data. Note that the percentage history contribution from the $\alpha F|F|$ term is most significant for $KC$ between 10 and 14 when the $MSE$ for the Morison fit is large. This range of $KC$ has particularly large lift forces [12] [13] which are caused by vortex shedding, providing qualitative evidence of the link between history and vortex shedding.

The values of the coefficients $C_m$, $C_d$ and $\alpha$ vary markedly from one situation to another and so we are clearly not providing a universal curve-fit equation. However, it is interesting to note that the sinusoidal case with $KC = 6.48$ and the De Voorst case with $KC = 5.03$ have very similar values for $C_m$ and $\alpha$ with different $C_d$'s, which is the only indication of the difference in $\beta$ values.

The force predictions of the model (7) gave little improvement on the Morison prediction due to bifurcation effects as described in [16].

These procedures worked correspondingly well on wave force and velocity data obtained from the Christchurch Bay Tower. These data were not so reliable as those measured in idealised situations but they gave at least a qualitative assessment of the procedures. A suitable sample was chosen for analysis and turned out to give a very severe test. The Morison fit was poor with the force peaks grossly underestimated. The history term gave a similar contribution to the drag in the predominat wave direction. On the basis of analysis in unidirectional flows, this indicates that the poor performance of Morison's equation is due to vortex shedding, a result that was not known *a priori*. The converse of the argument is that if a poor fit by the Morison equation is not associated with a significant history term then this is due to something other than vortex shedding.

# 3 System Identification via NARMAX Modelling

The previous section described an attempt to determine new model structures on heuristic physical grounds. Although the adoption of these new structures resulted in improved curve fits, predictions of the fluid forces were disappointing. (The important distinction between curve-fit accuracy and prediction accuracy as measures of model validity is discussed in more detail in [19].) The approach taken here is to allow sophisticated system identification techniques based on NARMAX models [8] free rein in deciding the appropriate terms for an extended model in an attempt to produce good fits and predictions. The extra terms produced may have no obvious relation to the flow phenomena involved.

The discrete Morison-Duffing equation of the last section is an example of a **NARMAX** model; the present sampled output $F_i$ is expressed as a nonlinear function of past inputs $u_{i-1}, \ldots, u_{i-n_u}$ and outputs $F_{i-1}, \ldots, F_{i-n_f}$. The most general polynomial NARMAX model (including products of order $\leq n_p$ but excluding noise modelling) is denoted by

$$F_i = F^{(n_p)}(F_{i-1}, \ldots, F_{i-n_f}; u_{i-1}, \ldots, u_{i-n_u}) \tag{8}$$

It has been proved [9] [10] under very mild assumptions that any input-output process has a representation by a model of the form (8). If the system nonlinearities are polynomial in nature, this model will represent the system well for all levels of excitation. If the system nonlinearities are not polynomial, they can be approximated arbitrarily accurately by polynomials over a given range of their arguments. Alternatively, a non-polynomial NARMAX model can be adopted.

In practice, it is unusual to know which terms should be in the model. This is not too much of a problem if the system under study is known to be linear; the number of possible terms is a linear function of the numbers of lags $n_f$, $n_u$. However, if the system is nonlinear, the number of possible terms increases *combinatorially* with increasing numbers of lags. In order to reduce the computational load on the parameter estimation procedure it is clearly desirable to determine which terms should be included. Also, experience indicates that a final model containing ten to fifteen terms is usually adequate. Because of this the NARMAX algorthms include a *structure detection* technique which determines automatically which terms should be in the model [19].

Having obtained a NARMAX model for a system, the next stage in the identification procedure is to determine if the structure is correct and the parameter estimates are unbiased. It is important to know if the model has successfully captured the system dynamics so that it will provide good predictions of the system output for different input excitations, or if it has simply fitted the model to the data; in which case it will be of little use since it will only be applicable to one data set. Three basic tests of the validity of a model are applied in the present work; two of the tests, the curve-fit or *one-step-ahead prediction* and the *model predicted output* are described in the previous section. The final and most stringent tests are the correlation tests [2] [19]. A number of correlation functions are required to vanish before one can infer model validity.

When the NARMAX routines were applied to the U-tube data described above, the resulting models were, for $KC = 11.88$

$$\begin{aligned} F_i = {} & 0.18021 \times 10 F_{i-1} - 0.78516 F_{i-2} - 0.41016 \times 10^{-1} F_{i-4} \\ & - 0.41113 u_{i-3} u_{i-3} u_{i-3} + 0.92188 u_i u_i u_i - 0.31250 F_{i-1} u_i u_i \\ & + 0.42653 \times 10^4 F_{i-4} u_{i-3} + 0.84966 \times 10^4 F_{i-4} u_i + 0.33159 \times 10^{-1} F_{i-1} F_{i-2} u_i \\ & - 0.12659 \times 10^5 F_{i-4} u_{i-1} \end{aligned} \tag{9}$$

for $KC$ =17.5,

$$\begin{aligned} F_i = {} & 0.16842 \times 10 F_{i-1} - 0.64108 F_{i-2} - 0.26385 \times 10^{-1} F_{i-1} F_{i-1} F_{i-1} \\ & - 0.80901 \times 10^{-1} u_i - 0.94940 \times 10^{-1} u_{i-2} + 0.83598 u_i u_i u_i \\ & - 0.58117 F_{i-3} u_{i-3} u_{i-3} + 0.14757 F_{i-2} F_{i-4} u_{i-3} \end{aligned} \tag{10}$$

and for $KC = 34.68$,

$$\begin{aligned} F_i = {} & 0.16968 \times 10 F_{i-1} - 0.92220 F_{i-2} + 0.62466 \times 10^{-1} F_{i-1} F_{i-1} F_{i-1} \\ & - 0.58983 u_{i-3} u_{i-3} u_{i-3} + 0.15208 \times 10 u_i u_i u_i - 0.80145 F_{i-1} u_i u_i \\ & + 0.46783 \times 10^{-2} F_{i-4} F_{i-4} + 0.22397 F_{i-3} - 0.33093 \times 10^{-1} u_{i-3} \end{aligned} \tag{11}$$

In each case, a substantial improvement over Morison's equation is obtained. To illustrate this, the model predicted output for the $KC = 11.88$ case is given in Figure 3. Note that the correlation functions

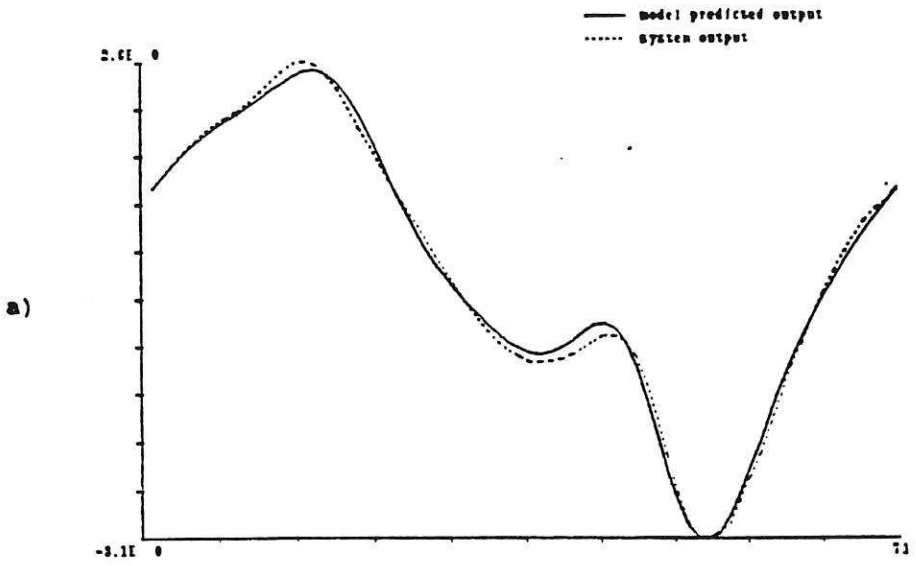


a)

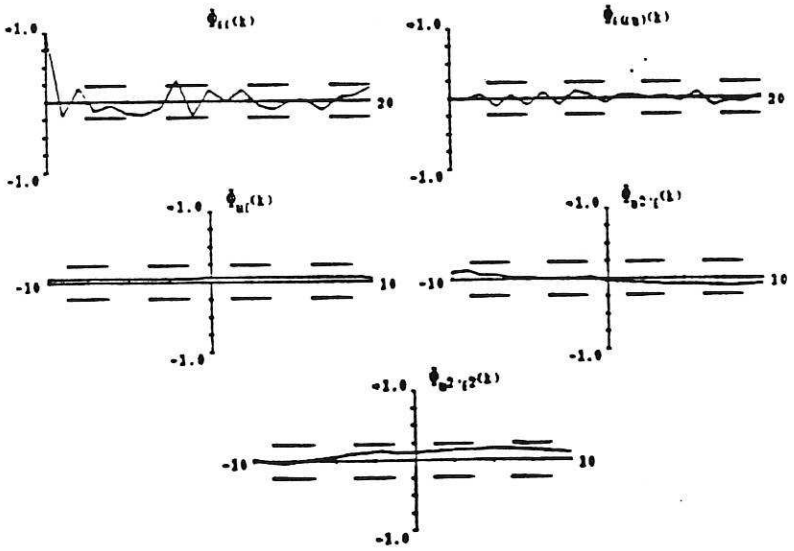

b)

**Figure 3.** NARMAX fit to $KC = 11.88$ U-tube data. (a) Model predicted output. (b) Correlation tests.

shown in Figure 3b are all within the 95% confidence limits (the dashed lines) for a null result. (The first of the correlation functions should actually be equal to 1 at the origin). In contrast, Morison's equation does not pass the correlation tests [19].

The number and type of the nonlinear terms changes for each data set. This is not particularly surprising if one assumes that no simple extension of the Morison equation exists; the cubic terms are always present because they are a part of the drag component, the source of the remaining nonlinearity is largely the vortex shedding as indicated in the previous section and it is well known that the pattern or mode of shedding can change dramatically as $KC$ changes.

A NARMAX analysis of the De Voorst data yielded the following model.

$$\begin{aligned} F_i &= 0.85124F_{i-1} - 0.29028F_{i-3} - 0.25433\times 10^2 u_{i-4} \\ &+ 0.73679\times 10^3 u_i - 0.71581\times 10^3 u_{i-1} + 0.47754\times 10^2 u_{i-4}u_{i-4}u_{i-4} \\ &+ 0.10364\times 10^{-2} F_{i-1}F_{i-1}u_{i-4} \end{aligned} \tag{12}$$

For the Christchurch Bay data, a complex model was obtained which included 29 terms most of which had no clear physical interpretation [19]. The fact that such a model was required can be offered in further support of the conclusion that the inadequacy of Morison's equation is due to the gross vortex shedding effects which were also observed in the U-tube experiments.

The results here seem to indicate that there is no simple extension to Morison's equation which allows a direct physical interpretation of the additional terms. The Christchurch Bay data shows a strong resemblance to the U-tube data in this respect.

# 4 Higher Order Frequency Response Functions

In the previous section, NARMAX methods were applied to force and velocity data for various flows around a cylinder. Although the resulting predictions gave substantial improvements over Morison's equation, the structures of the models differed for each flow. One reason why this situation might occur is that the discrete-time representation of a continuous-time system is not unique. In order to draw any conclusions from the NARMAX results in the time-domain, it is necessary to recover the underlying continuous-time model or use some other means which can reveal any common underlying physical structure in the NARMAX models. This can be done by passing to the frequency-domain where the system has a representation by a number of higher order frequency response functions (FRF's) which can be determined directly from the NARMAX representation [5].

The primary problem of system identification is to obtain a mathematical model of a given physical system from consideration of measured input and output data. In general mathematical terms, a system $S$ can be regarded as a *functional* which maps given input functions e.g. $x(t)$, to associated output functions $y(t)$.

$$y(t) = S[x(t)] \tag{13}$$

This is far too general to be very illuminating. However, it is well known that the input-output functional for a linear system can always be written in the form

$$y(t) = \int d\tau h(\tau - t)x(\tau) \tag{14}$$

a relationship which is sometimes referred to as Duhamel's integral. Within this framework, the system is specified uniquely by its Green's function or impulse response function $h(t)$. The Fourier transform $\mathcal{F}$ of equation (4.2) yields the familiar frequency domain expression

$$Y(\omega) = H(\omega)X(\omega) \tag{15}$$

where $X(\omega)$ and $Y(\omega)$ are the Fourier transforms of $x(t)$ and $y(t)$ respectively and $H(\omega) = \mathcal{F}[h(t)]$ is the system Frequency Response Function or FRF. All information about the system is encoded in either of the functions $h(t)$ and $H(\omega)$. Which representation is used in a given problem will usually be dictated by the form of the answer required.

Equations (14) and (15) are manifestly linear and therefore cannot hold for arbitrary nonlinear systems. However, both admit a generalisation. The extended form of equation (15) was obtained in the early part of this century by Volterra [17]. It takes the form of an infinite series

$$y(t) = y_1(t) + y_2(t) + y_3(t) + \cdots \tag{16}$$

where

$$y_1(t) = \int_{-\infty}^{+\infty} d\tau h_1(\tau) x(t-\tau) \tag{17}$$

$$y_2(t) = \int_{-\infty}^{+\infty}\int_{-\infty}^{+\infty} d\tau_1 d\tau_2 h_2(\tau_1,\tau_2) x(t-\tau_1)x(t-\tau_2) \tag{18}$$

$$y_3(t) = \int_{-\infty}^{+\infty}\int_{-\infty}^{+\infty}\int_{-\infty}^{+\infty} d\tau_1 d\tau_2 d\tau_3 h_2(\tau_1,\tau_2,\tau_3) x(t-\tau_1)x(t-\tau_2)x(t-\tau_3) \tag{19}$$

The form of the general term is obvious from the above. The functions $h_1(\tau)$, $h_2(\tau_1,\tau_2)$, $h_3(\tau_1,\tau_2,\tau_3)$, $\ldots h_n(\tau_1,\ldots,\tau_n)$, $\ldots$ are generalisations of the linear impulse response function and are usually referred to as *Volterra kernels*.

There exists a dual frequency-domain representation for nonlinear systems. The *higher order FRF's* or *Volterra kernel transforms* $H_n(\omega_1,\ldots,\omega_n)$, $n = 1,\ldots,\infty$ are defined as the multi-dimensional Fourier transforms of the kernels, i.e.

$$H_n(\omega_1,\ldots,\omega_n) = \int_{-\infty}^{+\infty}\ldots\int_{-\infty}^{+\infty} d\tau_1\ldots d\tau_n h_n(\tau_1,\ldots,\tau_n) e^{-i(\omega_1\tau_1+\ldots+\omega_n\tau_n)} \tag{20}$$

$$h_n(\tau_1,\ldots,\tau_n) = \frac{1}{(2\pi)^n}\int_{-\infty}^{+\infty}\ldots\int_{-\infty}^{+\infty} d\omega_1\ldots d\omega_n H_n(\omega_1,\ldots,\omega_n) e^{+i(\omega_1\tau_1+\ldots+\omega_n\tau_n)} \tag{21}$$

The frequency-domain dual of the expression (17) is

$$Y(\omega) = Y_1(\omega) + Y_2(\omega) + Y_3(\omega) + \ldots \tag{22}$$

where

$$Y_1(\omega) = H_1(\omega)X(\omega) \tag{23}$$

$$Y_2(\omega) = \frac{1}{2\pi}\int_{-\infty}^{+\infty} d\omega_1 H_2(\omega_1,\omega-\omega_1)X(\omega_1)X(\omega-\omega_1) \tag{24}$$

$$Y_3(\omega) = \frac{1}{(2\pi)^2}\int_{-\infty}^{+\infty}\int_{-\infty}^{+\infty} d\omega_1 d\omega_2 H_3(\omega_1,\omega_2,\omega-\omega_1-\omega_2)X(\omega_1)X(\omega_2)X(\omega-\omega_1-\omega_2) \tag{25}$$

As for a linear system, the choice of time or frequency-domain representation is largely dictated by the problem. In this case, the frequency-domain is indicated for the following reason. The objects under study are the NARMAX models shown in the previous section. It was observed there that time-domain models for two similar flows might contain different model terms. Because the NARMAX representation of a system is not unique, one cannot be sure if differences in the model structures for different flows are due to differences in the underlying physics or simply a reflection of the non-uniqueness. However, the non-uniqueness is not a problem in the frequency-domain. No matter what the form of the model, if it represents the measured data accurately it must reflect the correct frequency content, both from linear and nonlinear parts of the system.

If one knows the equation of motion of a system (differential or discrete), the method of harmonic probing can be used to obtain exact expressions for the higher order FRF's. The method was introduced in [1] for systems with continuous-time equations of motion and extended to discrete-time systems in [5].

The validation and interpretation of the higher order FRF's is discussed in detail in [19]. Briefly, just as the graph of $H_1(\omega)$ as a function of $\omega$ gives a curve which characterises a given linear system. A nonlinear system would also have a $H_2(\omega_1,\omega_2)$ *surface* defined over the $(\omega_1,\omega_2)$ plane which characterises the second order nonlinear behaviour. In much the same way as peaks in $H_1(\omega)$ indicate the frequencies at which elevated levels of output or resonances would be expected, ridges in the $H_2$ surface give information about which combinations of frequencies will boost the second order component of the output $y_2(t)$. The same is true for $H_3$ which gives information about combinations of three frequencies. A problem arises in the display of the FRF's of above second order, the surfaces exist in four dimensions or more; the solution to the problem adopted here is to plot the restriction $H_3(\omega_1,\omega_2,\omega_2)$ over the $(\omega_1,\omega_2)$ plane.

Having reviewed the appropriate machinery for generating and interpreting higher order FRF's, it can now be applied to Morison's equation. One slight complication arises; for technical reasons [19] it is neccessary to expand the drag term $u(t)|u(t)|$ as a polynomial. To third order, Morison's equation is

$$F(t) = K_d^{(1)}u + K_d^{(3)}u^3 + K_m\dot{u} \tag{26}$$

in a convenient shorthand. Application of the harmonic probing algorithm yields the FRF's

$$H_1(\omega) = K_d^{(1)} + iK_m\omega \tag{27}$$

$$H_3(\omega_1,\omega_2,\omega_3) = \frac{1}{6}K_d^{(3)} \tag{28}$$

The second order FRF vanishes as a consequence of the fact that nonlinearity is an odd power. This is not due to the approximation procedure; $u|u|$ is an odd function so any least-squares polynomial approximation will also be odd.

The third order FRF for the approximate Morison system is simply a constant, all components in the third order output $y_3(t)$ appear with the same amplitude independently of input frequencies; therefore there are no third order 'resonances'.

Having obtained the higher order FRF's, one can substitute into equations (23) and (25) and thence into (22) to obtain the nonlinear spectral representation of the force in terms of the velocity spectrum $U(\omega)$

$$F(\omega) = (K_d^{(1)} + iK_m\omega)U(\omega) + \frac{K_d^{(3)}}{24\pi^2}U * U * U(\omega) \tag{29}$$

where $*$ denotes a convolution product.

This type of equation was introduced in [18]; a study of the efficacy of this equation based on experimental data obtained in the De Voorst wave flume is presented in [7].

It is only a little more difficult to determine the higher order FRFs for the Morison-Duffing equation (6) which was examined above as a possible extension to Morison's equation. On approximating the $u|u|$ and $F|F|$ terms by cubics one obtains

$$F_i = a_1F_{i-1} + a_2F_{i-2} + a_3F_{i-1}^3 + b_1u_{i-1} + b_2u_{i-2} + b_3u_{i-1}^3 \tag{30}$$

where $a_1, a_3, b_1$ and $b_3$ are now functions of the approximating intervals. Harmonic probing of this system yields the higher order FRF's

$$H_1(\omega) = \frac{b_1e^{-i\omega\Delta t} + b_2e^{-2i\omega\Delta t}}{1 - a_1e^{-i\omega\Delta t} - a_2e^{-2i\omega\Delta t}} \tag{31}$$

$$H_3(\omega_1,\omega_2,\omega_3) = \frac{1}{2}\frac{e^{-i(\omega_1+\omega_2+\omega_3)\Delta t}(a_3H_1(\omega_1)H_1(\omega_2)H_1(\omega_3) + b_3)}{1 - a_1e^{-i(\omega_1+\omega_2+\omega_3)\Delta t} + a_2e^{-2i(\omega_1+\omega_2+\omega_3)\Delta t}} \tag{32}$$

This equation has much more complex third order dynamics. $H_3$ for the $KC = 17.5$ U-tube data is given in Figure 4. Note the prominent ridges in the magnitude plot, these correspond to nonlinear resonance conditions for combinations of three input frequencies. The form of the $H_3$ differs greatly from that for Morison's equation which is simply a flat plane.

As the basic NARMAX models for the flows examined had different structures, the algebraic forms for the higher order kernels also differ. For example the $KC = 17.5$ U-tube model (10) produced the forms

$$H_1(\omega) = \frac{b_0 + b_2e^{-2i\omega\Delta t}}{1 - a_1e^{-i\omega\Delta t} - a_2e^{-2i\omega\Delta t}} \tag{33}$$

and

$$6H_3(\omega_1,\omega_2,\omega_3)\{1 - a_1e^{-i(\omega_1+\omega_2+\omega_3)\Delta t} - a_2e^{-2i(\omega_1+\omega_2+\omega_3)\Delta t}\} =$$

$$3c_1e^{-i(\omega_1+\omega_2+\omega_3)\Delta t}H_1(\omega_1)H_1(\omega_2)H_1(\omega_3) + c_2 + c_3e^{-3i(\omega_1+\omega_2+\omega_3)\Delta t}(H_1(\omega_1) + H_1(\omega_2) + H_1(\omega_3)) +$$

$$c_4\{e^{-i(2\omega_1+4\omega_2+3\omega_3)\Delta t}H_1(\omega_1)H_1(\omega_2) + e^{-i(3\omega_1+2\omega_2+4\omega_3)\Delta t}H_1(\omega_2)H_1(\omega_3) + e^{-i(4\omega_1+3\omega_2+2\omega_3)\Delta t}H_1(\omega_1)H_1(\omega_3)\} \tag{34}$$

while the De Voorst model (12) gave

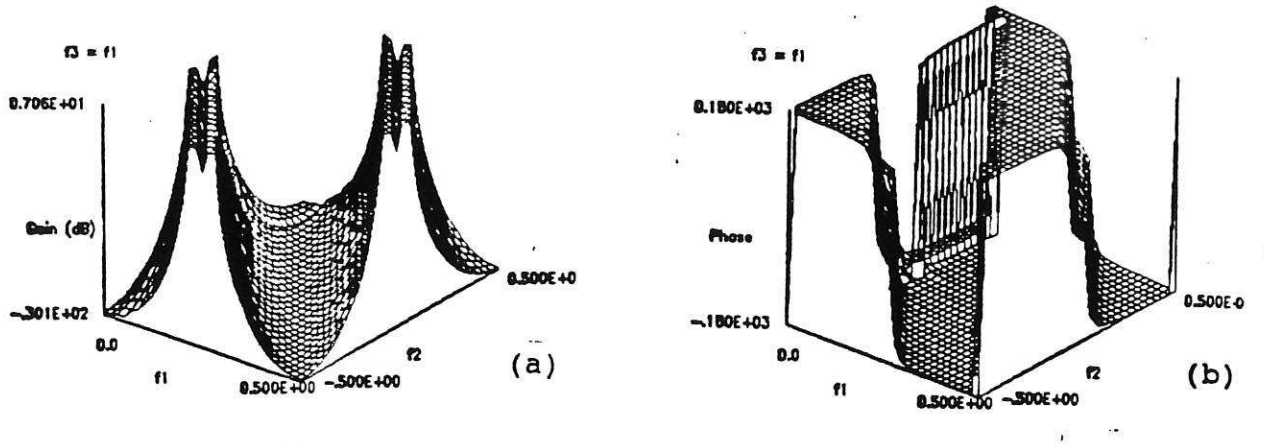


Figure 4. $H_3(\omega_1, \omega_2, \omega_1)$ from Morison-Duffing fit to U-tube data with $KC = 17.5$. (a) Magnitude. (b) Phase.

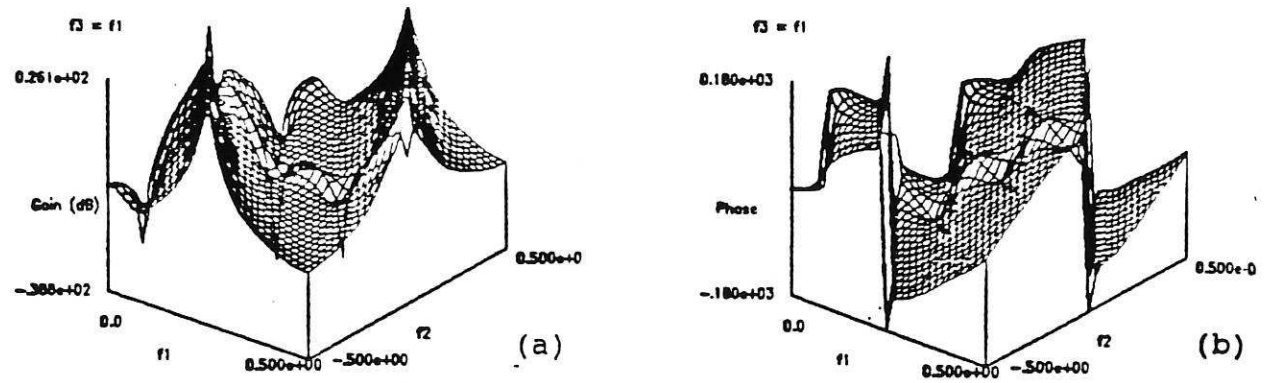


Figure 5. $H_3(\omega_1, \omega_2, \omega_1)$ from NARMAX fit to U-tube data with $KC = 17.5$. (a) Magnitude. (b) Phase.

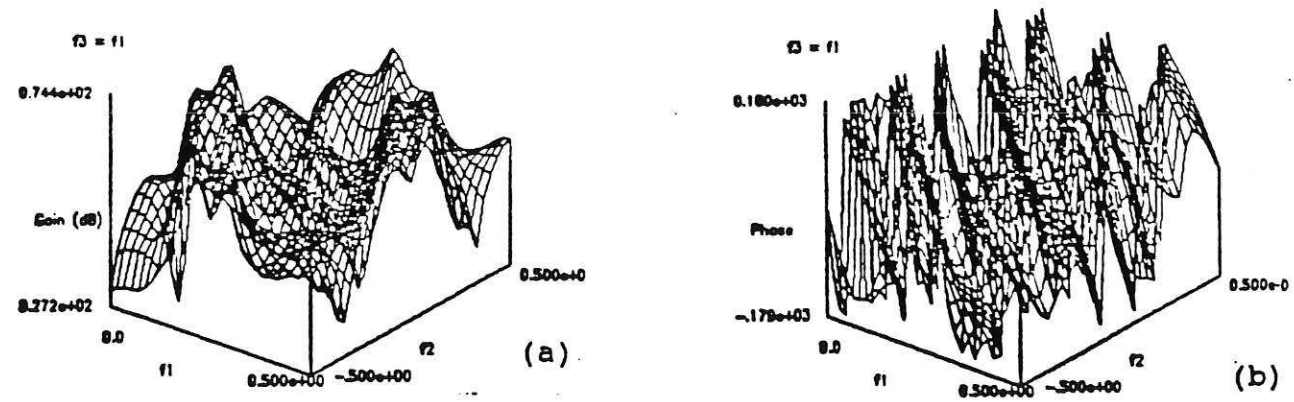


Figure 6. $H_3(\omega_1, \omega_2, \omega_1)$ from NARMAX fit to De Voorst data with $KC = 17.5$. (a) Magnitude. (b) Phase.

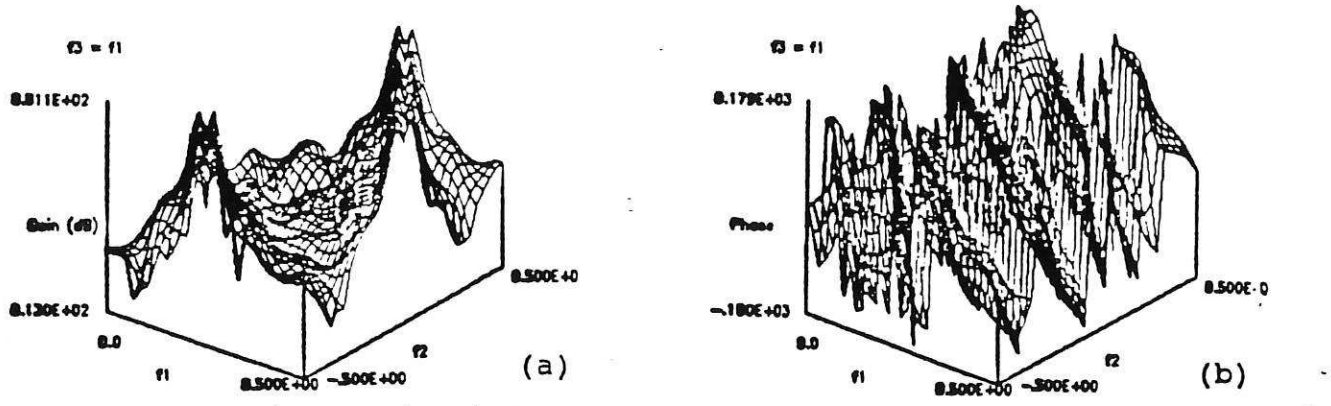


Figure 7. $H_3(\omega_1, \omega_2, \omega_1)$ from NARMAX fit to Christchurch Bay data with $KC = 17.5$. (a) Magnitude. (b) Phase.

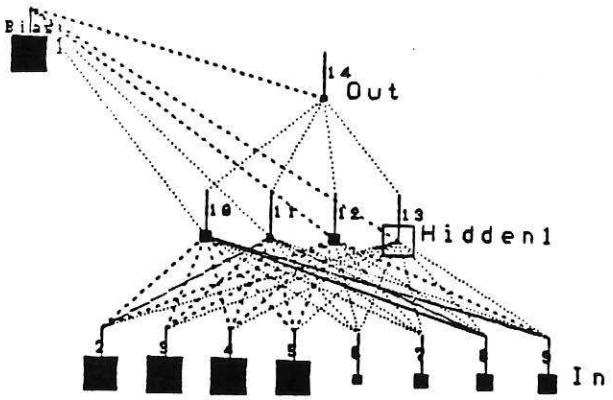


Figure 8. Neural network for force prediction.

$$H_1(\omega) = \frac{b_0 + b_1 e^{-i\omega\Delta t} + b_4 e^{-4i\omega\Delta t}}{1 - a_1 e^{-i\omega\Delta t} - a_3 e^{-3i\omega\Delta t}} \tag{35}$$

and

$$6H_3(\omega_1,\omega_2,\omega_3)\{1 - a_1 e^{-i(\omega_1+\omega_2+\omega_3)\Delta t} - a_3 e^{-3i(\omega_1+\omega_2+\omega_3)\Delta t}\} = c_1 e^{-4i(\omega_1+\omega_2+\omega_3)\Delta t} +$$

$$c_2 e^{-i(\omega_1+\omega_2+\omega_3)\Delta t}\{e^{-3i\omega_3\Delta t}H_1(\omega_1)H_1(\omega_2) + e^{-3i\omega_2\Delta t}H_1(\omega_1)H_1(\omega_2) + e^{-3i\omega_3\Delta t}H_1(\omega_1)H_1(\omega_2)\} \tag{36}$$

where the $a$ and $b$ coefficients correspond to the linear terms and the $c$ coefficients to the nonlinear terms. Although the structures for the $H_3$'s are quite different they both produce the same features in the frequency domain (Figures 5 and 6). Both contain the characteristic ridges which were also present in the $H_3$ for the Morison-Duffing equation. In fact these ridges occur in all the U-tube $H_3$'s and also in the $H_3$ derived by NARMAX analysis of the Christchurch Bay data (Figure 7) [19]. The similarity between all the measured $H_3$'s and that of the Morison-Duffing equation suggests that the Morison-Duffing form could be curve-fitted to the experimental data yielding, via equations (22), (23) and (25), an expression for the nonlinear force spectrum which generalises (29). The fact that a model equation cannot predict accurately in the time-domain should not matter as long as the algebraic structure which results for $H_3$ is sufficiently flexible to represent the various cases; the Morison-Duffing structure shows promise in this respect. It is significant that all the data so far examined shows a definite third order structure which is not predicted by Morison's equation.

# 5 Neural Networks

A recent development in system identification is the use of neural networks to model dynamical systems [3]. A very brief description of one form of neural network, the multi-layer perceptron (MCP), is given here; many other network paradigms exist [14].

The MCP is simply a collection of connected processing elements called nodes arranged together in layers (Figure 8). A set of signal values pass into the *input layer* nodes, progress forward through the network *hidden layers* and the result finally emerges through the *output layer*. Each node $i$ is connected to each node $j$ in the preceding and following layers through a connection of weight $w_{ij}$. Signals pass through the node as follows: a weighted sum is performed at $i$ of all the signals $x_j$ from the preceding layer, giving the excitation $z_i$ of the node, this is then passed through a nonlinear *activation function* $f$ to emerge as the output of the node $x_i$ to the next layer i.e.

$$x_i = f(\sum_j w_{ij} x_i) \tag{37}$$

Various choices for the function $f$ are possible, the one adopted here is the hyperbolic tangent function $f(x) = \tanh(x)$. One node of the network, the *bias* node is special in that it is connected to all other nodes in the hidden and output layers, the output of the bias node is held constant throughout in order to allow constant components in the excitations $z_i$ of each node.

The first stage of using a network to model an input-output system is to establish the appropriate values for the connection weights $w_{ij}$. This is the *training* or *learning* phase. Training makes use of a set of network inputs for which the desired network output is known; at each training step, a set of inputs are passed forward through the network yielding a trial output, this is compared with the desired output. If the comparison error is considered small enough, the weights are not adjusted. If however a significant error is obtained, the error is passed *backwards* through the net and a *training algorithm* is used to adjust the connection weights as the error signal propagates back through the hidden layers. The algorithm used in this work is the *backpropagation* algorithm. A detailed mathematical description can be found in [14]. Once the comparison error is reduced to an acceptable level over the whole training set, the training phase ends and the network is established. The networks used in the following were designed and trained using the NeuralWorks Professional II package produced by NeuralWare Ltd.

The neural network presented here was trained to predict the force time-history for sampled data from the U-tube experiments described above with $KC = 6.48$. A Morison equation fit to this data yielded a prediction $MSE$ of 0.42 (Figure 9). A neural network was chosen with an input layer containing 8 nodes, a single hidden layer containing 4 nodes and an output layer consisting of a single node. The values presented to the input layer at each sampling instant were the past 4 values of velocity and force i.e. $u_{i-1},\ldots,u_{i-4},F_{i-1},\ldots,F_{i-4}$; the desired output being the present value of the force $F_i$. After

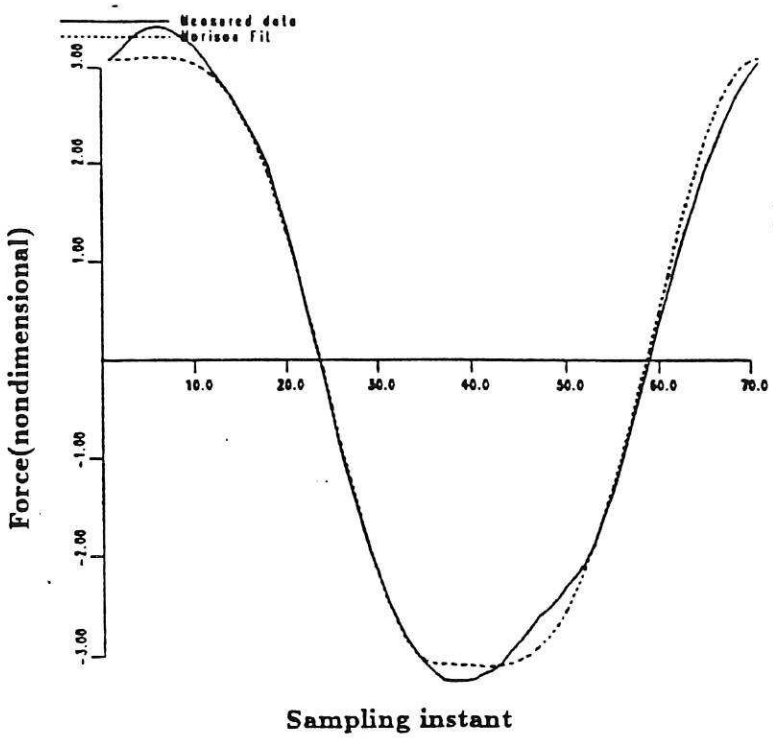


**Figure 9.** Comparison between measured U-tube data and Morison equation prediction. $KC = 6.48$.

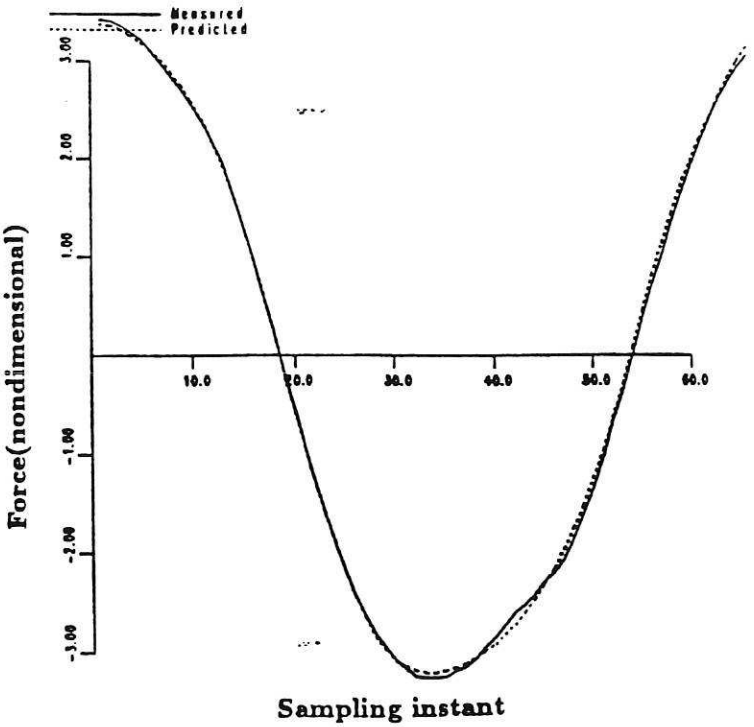


**Figure 10.** Comparison between measured U-tube data and neural network prediction. $KC = 6.48$.

training, with the weight values established, the network furnished a representation of the velocity-force system

$$F_i = F(u_{i-1}, \ldots, u_{i-4}, F_{i-1}, \ldots, F_{i-4}) \tag{38}$$

and this is little more than a highly non-polynomial NARMAX model. After training on the U-tube data, the network was used to predict the force, the result is shown in Figure 10. The $MSE$ for the prediction was 0.042, which is a factor of ten reduced from the Morison prediction. The neural network offers hope of accurate force predictions, the non-polynomial nature of the system is not a disadvantage as there is little reason to suppose that the underlying physics of the vortex shedding mechanism should be expressible in polynomial terms. Work is currently in progress on obtaining prediction networks for a range of flows, the ultimate aim being to model a directional sea.

# Conclusions

A number of contempory signal processing techniques have been applied to the problem of modelling wave forces. Results include an improved classification of wave forces and accurate prediction models based on NARMAX analysis and neural networks. However, the models which predict accurately are case specific and this limits the usefulness of the time-domain approach.

Through the Duffing-Morison equation an algebraic structure is proposed for the higher order FRF's which appears flexible enough to cover all cases of interest to a degree of approximation; further work is required. On substituting into a series expansion for the force spectrum this would allow a more accurate model of high frequency components in the signal. This clearly has implications for fatigue analysis.

# Acknowledgements

Thanks are due to Delft Hydraulics for access to the wave force data obtained in the Delta flume in their De Voorst facility. This data was provided with the assistance of Malcolm Birkinshaw of the Health and Safety Executive and Professor Peter Bearman and Martin Davies of Imperial college. In particular, the help provided by Martin Davies in translating data into a useful format is much appreciated. Thanks are also due to Dr. Emmanuel Obasaju for making available unpublished data from his experimental work undertaken as a research associate at Imperial College. This project was supported by the Offshore Safety Division of the Health and Safety Executive through the Marine Technology Directorate's managed programme on the Behaviour of Fixed and Compliant Offshore Structures which is also sponsored by SERC, Amoco, BP, Elf, Statoil, Admiralty Research Establishment, Brown and Root Marine and Aker Engineering.

# References

[1] Bedrossan (E.) & Rice (S.O.) 1971 *Proceedings IEEE* **59** pp.1688-1707. The output properties of Volterra systems driven by harmonic and Gaussian inputs.

[2] Billings (S.A.), Chen (S.) & Backhouse (R.J.) 1989 *Journal of Mechanical Systems and Signal Processing* **3** pp.123-142. Identification of linear and nonlinear models of a turbocharged automotive diesel engine.

[3] Billings (S.A.), Jamaluddin (H.B.) & Chen (S.) 1992 *International Journal of Control* **55** pp.193-224. Properties of neural networks with applications to modelling non-linear dynamical systems.

[4] Billings (S.A.) & Tsang (K.M.) 1989 *Mechanical Systems and Signal Processing* **3** pp.319-339. Spectral analysis for nonlinear systems, part I: Parametric non-linear spectral analysis.

[5] Billings (S.A.) & Tsang (K.M.) 1989 *Mechanical Systems and Signal Processing* **3** pp.341-359. Spectral analysis for nonlinear systems, part II: Interpretation of nonlinear frequency response functions.

[6] Bishop (J.R.) 1979 *National Maritime Institute report no. NMI R57* Aspects of large scale wave force experiments and some early results from Christchurch Bay.

[7] Bliek (A.) & Klopman (G.) 1988 *proceedings of BOSS 1988* pp.821-840. Non-linear frequency modelling of wave forces on large vertical and horizontal cylinders in random waves.

[8] Chen (S.), Billings (S.A.) & Liu (Y.P.) 1987 *International Journal of Control* **50** pp.1873-1896. Orthogonal least-squares methods and their application to nonlinear system identification.

[9] Leontaritis (I.J.) & Billings (S.A.) 1985 *International Journal of Control* **41** pp.303-328. Input-output parametric models for Nonlinear systems. Part I: deterministic nonlinear systems.

[10] Leontaritis (I.J.) & Billings (S.A.) 1985 *International Journal of Control* **41** pp.329-344. Input-output parametric models for Nonlinear systems. Part II: stochastic nonlinear systems.

[11] Morison (J.R.), O'Brien (M.P.), Johnson (J.W.) & Schaf (S.A.) 1950 *Petroleum Transactions* **189** pp.149-157. The force exerted by surface waves on piles.

[12] Obasaju (E.D.), Bearman (P.W.) & Graham (J.M.R.) 1988 *Journal of Fluid Mechanics* **196** pp.467-494. A study of forces, circulation and vortex patterns around a circular cylinder in oscillating flow.

[13] Obasaju (E.D.), Bearman (P.W.) & Graham (J.M.R.) 1991 Proceedings of the First ISOPE conference, Edinburgh 1991 Vol.III pp.340-345. In-line forces on a cylinder performing large amplitude oscillation in a steady current.

[14] Rumelhart (D.E.) & McClelland (J.L.) 1988 *Parallel Distributed Processing: Explorations in the Microstructure of Cognition (Two Volumes)*. MIT press.

[15] Sarpkaya (T.) 1981 *US Naval Civil Engineering Laboratory Report no. CR 82.008*. Morison's equation and the wave forces on offshore structures.

[16] Stansby (P.K.), Worden (K.), Billings (S.A.) & Tomlinson (G.R.) 1992 *to appear in Applied Ocean Research*. Improved wave force classification using system identification.

[17] Volterra (V.) 1959 *Theory of Functionals and Integral equations*. Dover Publications, New York.

[18] Vugts (J.H.) & Bouquet (A.G.) 1985 *Proceedings of BOSS 1985 - Delft* pp239-253. A non-linear frequency domain description of wave forces on an element of a vertical pile in random seas.

[19] Worden (K.), Billings (S.A.), Stansby (P.K.) & Tomlinson (G.R.) 1992 *Analysis of Wave Forces Using System Identification*. To be published by HMSO.